ACS OMEGA

http://pubs.acs.org/journal/acsodf

Article

Ferric Chloride-Induced Synthesis of Silver Nanodisks with Considerable Activity for the Reduction of 4-Nitrophenol

Jie Chen, Linlin He, Zhengyang Fan, Hongwei Yang,* Huaming Mao, Yu Ren, Jungang Yin, Wei Dai, and Hao Cui*

Cite This: *ACS Omega* 2022, 7, 28860−28865

Read Online

ACCESS | Metrics & More | Article Recommendations | Supporting Information

ABSTRACT: Silver nanodisks (AgNDs) have been successfully synthesized by using ferric chloride as an auxiliary agent in the presence of polyvinylpyrrolidone and *N*,*N*-dimethylformamide as both a solvent and a reducing agent. The mass ratio of reactants, temperature, and time were demonstrated to be the key factors determining the morphology of the product, and the conversion of Fe^{3+}/Fe^{2+} ions played an important role in increasing the ratio of silver nanosheets (AgNSs). As the reaction prolonged, the etching effect of Cl^- ions on the tips of AgNSs became more and more obvious, which made the obtained typical polygonal AgNSs turn into AgNDs eventually. In addition, the prepared AgNDs exhibited a considerable catalytic activity in the reduction of 4-nitrophenol.

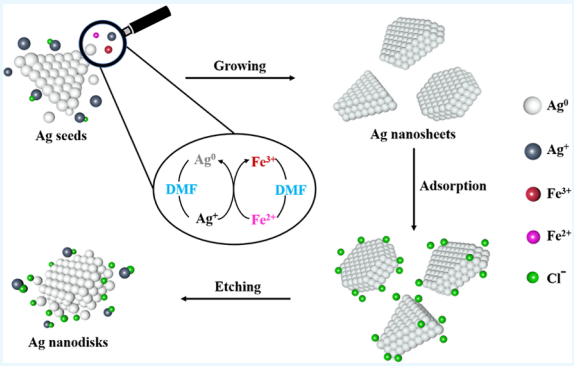

1. INTRODUCTION

Metal nanomaterials have received extensive attention due to their unique properties and potential applications in the fields of biology, medicine, optics, sensing, and catalysis.[1−5] A variety of methods have thus been developed for the synthesis of metal nanomaterials with different shapes.[6−8] Among these metal nanomaterials, silver nanosheets (AgNSs) with a controllable shape, size, and thickness have attracted extensive research interest in recent years due to their novel two-dimensional structure and related applications.

To date, the strategies for the synthesis of AgNSs mainly include the solvothermal method, photochemical method, chemical reduction method, seed-mediated growth method, template-oriented growth method, and so on.[9,10] For instance, in the presence of cyanuric acid, Kim et al. synthesized zigzag-shaped AgNSs with high lateral dimensions by the solvothermal method. The strain sensor made by adding these AgNSs showed extremely high sensitivity and high ductility.[11] Weng and his co-workers adopted a chemical reduction method to prepare AgNSs and found that silver triangular nanosheets with different concentrations and sizes had different surface-enhanced Raman scattering activities.[12] Khan et al. introduced a seed-mediated growth method without polyvinylpyrrolidone (PVP) to synthesize AgNSs that resonated in the near-infrared range. In this method, silver seed crystals could gradually grow into AgNSs with a size of 100−600 nm within a few minutes.[13]

Among the above methods, the solvothermal method is relatively simple, but the choice of solvent is critical.[14,15] Thus far, various solvents have been applied for the synthesis of AgNSs. For example, Neethu et al. used an organic solvent (*N*-2-methyl pyrrolidone) as the solvent, which is structurally similar to PVP, providing good kinetic control to tune the edge length of Ag nanosheets.[16] Xia and his co-workers reported that Ag nanosheets can be obtained with yields as high as 90% in ethylene glycol by simply introducing polyacrylamide into the synthesis.[17] Kim's group introduced the role of PVP in their method. In *N*,*N*-dimethylformamide (DMF), PVP reduces the silver salt at a slow rate, so the growth process of nanoparticles is controlled by kinetics, finally forming AgNSs.[18] It is worth noting that AgNSs reported in previous studies were usually of a typical polygonal shape, and the one-step synthesis of rounded AgNSs, called AgNDs, was seldom reported until now.

4-nitrophenol (4-NP) is a highly toxic and harmful water pollutant, but its reduced product 4-aminophenol (4-AP) is a common pharmaceutical ingredient.[19−21] Therefore, it is believed that direct reduction of 4-NP to 4-AP under the action of a catalyst is a more effective and environmentally friendly method.[22,23] Commonly, the performance of a catalyst is closely related to its morphology and size. Specially, silver multi-dimensional nanomaterials often have high catalytic

Received: March 29, 2022
Accepted: August 3, 2022
Published: August 12, 2022

capabilities due to their large specific surface area and more exposed active sites.[24,25]

Herein, AgNDs have been synthesized one step via a simple solvothermal method by using $FeCl_3$ as an auxiliary agent and DMF as both a solvent and a reductant. Further, the possible growth mechanism of AgNDs was proposed. In particular, the prepared AgNDs exhibited a considerably high catalytic activity for the reduction of 4-NP.

2. EXPERIMENTAL SECTION

2.1. Materials. Silver nitrate ($AgNO_3$, ≥99.8%), ethanol (C_2H_5OH, ≥99.7%), ethylene glycol ($(CH_2OH)_2$, ≥99.5%), and PVP (PVP-K30, M_w = 45000) were purchased from Sinopharm Chemical Reagent Co., Ltd. Iron(III) chloride anhydrous ($FeCl_3$, ≥99.9%), ferrous chloride ($FeCl_2$, ≥99.9%), ferric nitrate nonahydrate ($Fe(NO_3)_3{\cdot}9H_2O$, ≥98.5%), and DMF (≥99.5%) were purchased from Sigma Aldrich. All chemicals were used as received without further purification.

2.2. Methods. *Synthesis of AgNSs and AgNDs.* In a typical synthetic route, $FeCl_3$, $AgNO_3$, and PVP were added and dissolved in sequence into 20 mL of DMF in a small beaker under ultrasonic vibration. All chemicals were used as received without further purification. Then, the mixture was transferred to an autoclave lined with polytetrafluoroethylene and kept at a temperature for a specific time. When the autoclave was naturally cooled down to room temperature, the product was taken out, centrifuged, and washed using an appropriate amount of ethanol several times. Eventually, the samples obtained after 9 and 12 h of the reaction were named AgNSs and AgNDs, respectively.

2.3. Characterization. The size and morphology of AgNSs and AgNDs were characterized by scanning electron microscopy (SEM) (Hitachi S-3400N). The elemental composition of the sample was analyzed using an energy spectrometer. A UV−vis spectrophotometer (PERSIE Genera TU-1901) was used to monitor the UV−vis spectra of synthesized AgNSs and AgNDs. X-ray diffraction (XRD) was used for phase identification with the Cu target and K_α radiation (λ = 1.54056 Å), where the scanning range (2θ) was 20 to 90°, and the step size was 0.02°. Transmission electron microscopy (TEM) was carried out on a JEM-2100 microscope (200 kV, Cs = 1.35 mm) with a voltage of 120 kV. The specific surface area was analyzed using a micromeritics Gemini-VII2390 and calculated by the Brunauer−Emmett−Teller (BET) method.

3. RESULTS AND DISCUSSION

In this study, the samples prepared at different temperatures, times, and raw material ratios were studied, from which the optimal experimental conditions were obtained (Table S1 and Figure S1). It is found that the ratio of AgNSs in the product could reach as high as over 90% when the reaction occurred at 423 K for 9 h as the mass ratio of $AgNO_3$/PVP/$FeCl_3$ was 1:0.9:0.04. It is clear that the obtained AgNSs have visible corners and sizes of a sub-micron level. To verify the role of $FeCl_3$ in the synthesis of AgNDs, we compared not only the products obtained without additives at 423 K for 12 h but also the products obtained with $Fe(NO_3)_3{\cdot}9H_2O$ and $FeCl_2$ as additives under the same conditions, respectively. It can be found from Figure 1 that Fe^{3+} ions can indeed promote the synthesis of AgNSs. In detail, we have tried to use the same amount of deionized water and ethylene glycol as the solvent instead of DMF, and the reaction was carried out under the same conditions. The related results are shown in Figure S2a,b, respectively. Figure S2a shows that the product mainly consists of particles, while Figure S2b reveals that coarse silver nanorods and many irregular particles are produced in the ethylene glycol system. These results indicate that DMF is necessary for the synthesis of AgNSs in this work.

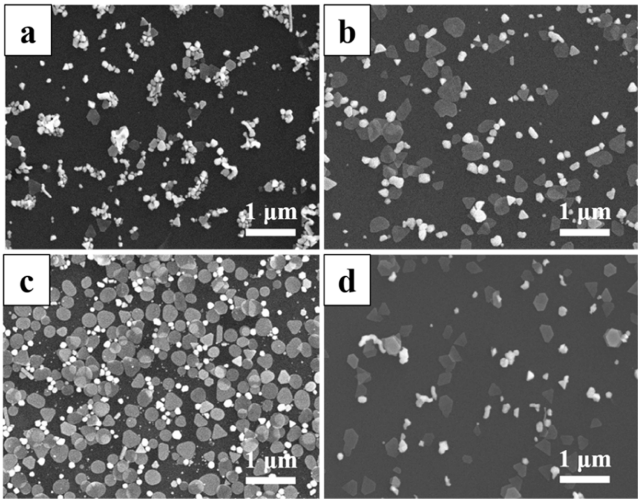

Figure 1. SEM images of the samples prepared under 423 K for 12 h (a) without additives, (b) with ferric nitrate nonahydrate, (c) with ferric chloride, and (d) with ferrous chloride.

In order to investigate the morphology evolution of AgNDs during the reaction, both the time-dependent SEM and UV−vis characterizations were carried out, and the results are presented in Figure 2. It can be observed that AgCl particles formed at the beginning of the reaction according to the inserted elemental analysis diagram in Figure 1a. As the reaction time prolonged to 3 h, AgCl particles were gradually consumed into small particles and AgNSs began to appear. With the increase of the reaction time from 6 h up to 12 h gradually, the corners of AgNSs were continuously passivated and eventually turned into quasi-circular AgNDs (Figure 2b−e).

The UV−vis spectra of samples prepared at different stages are shown in Figure 2f, and the inset is a partially enlarged image in the wavelength range of 320−520 nm. It is clear that with the increase of the reaction time, there is an increasingly broad peak between 340 and 470 nm, which should be caused by the out-of-plane quadrupole plasmon resonance, the out-of-plane dipole plasmon resonance, and the in-plane quadrupole plasmon resonance of AgNSs.[26] When the reaction time reaches up to 12 h, the sharp corners of AgNSs are etched into round corners, and the peaks of AgNDs tend to become flat. On the other hand, since the average grain sizes of AgNSs and AgNDs are ∼500 nm, the in-plane dipole plasmon resonance peaks sensitive to the grain size are not detected in this work.[27]

Based upon the above results and discussions, a possible growth mechanism of AgNDs was proposed, as illustrated in Figure 3. According to the calculation of the Nernst equation, the reduction electrode potential of Fe^{3+}/Fe^{2+} is higher than that of $AgCl/Ag^0$, and Fe^{3+} will be preferentially reduced to Fe^{2+} by DMF in the reaction system.[28,29] As the reaction proceeds, under the synergetic reduction of DMF and Fe^{2+} ions, Ag^+ ions are gently reduced into Ag^0 atoms and formed silver seed crystals, which further promote the forward

https://doi.org/10.1021/acsomega.2c01928
ACS Omega 2022, 7, 28860−28865

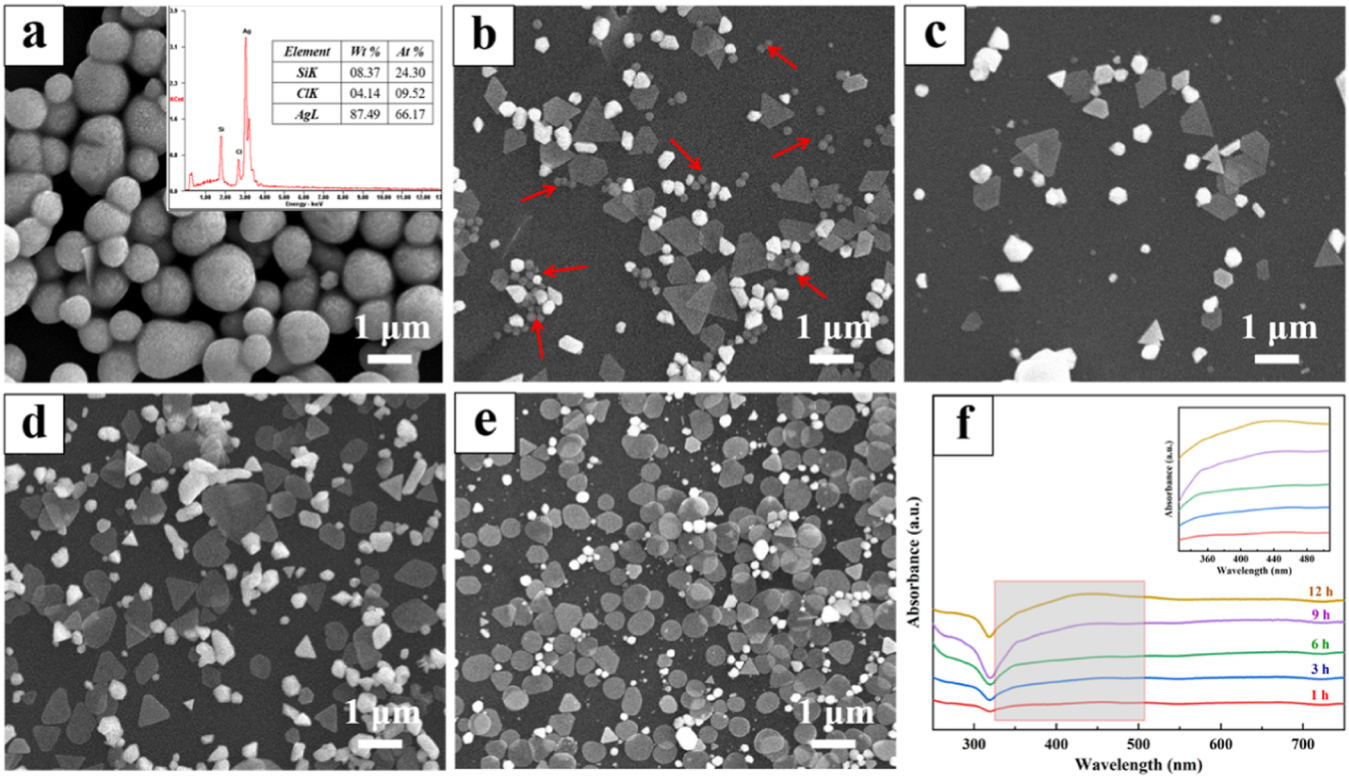

Figure 2. SEM images of the samples prepared at different stages: (a) 1 h and the illustration is its elemental analysis diagram, (b) 3 h, (c) 6 h, (d) 9 h, and (e) 12 h; (f) UV−vis spectra of samples prepared in a−e.

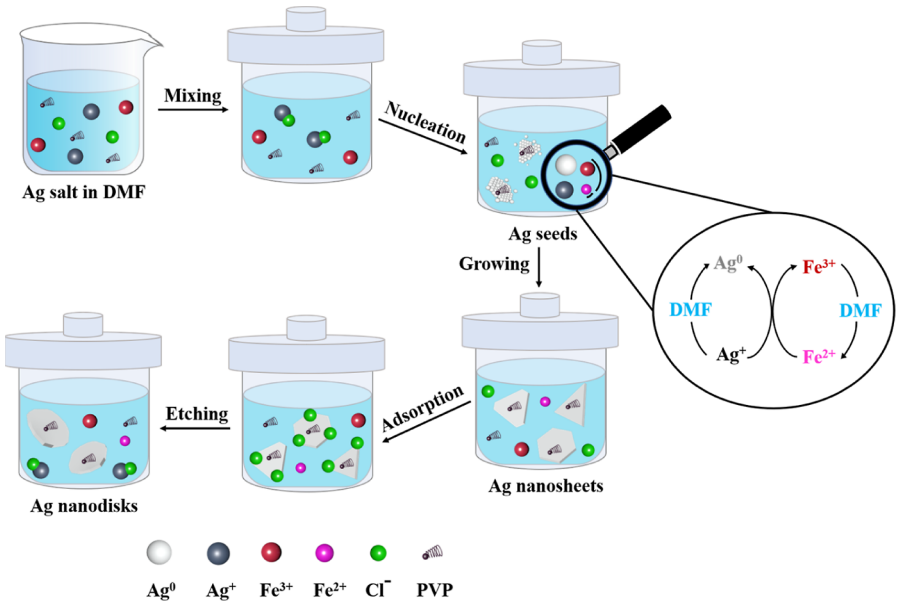

Figure 3. Schematic diagram of the possible growth mechanism of AgNDs.

reaction, and AgCl particles continuously release Ag^+ ions and Cl^- ions. Meanwhile, the PVP molecules can directionally adsorb onto the Ag(111) crystal plane and hinder its growth, thus promoting the formation of polygonal AgNSs eventually. In contrast, the silver seed crystals without the action of PVP molecules tend to grow into irregular particles.[30] When the reaction proceeds to a certain stage, the Cl^- ions in the solution become overmuch. As reported in previous studies, the etching ability of different halide ions on AgNSs was calculated by the activation energy of etching reaction as $Cl^- < I^- < Br^-$.[31] The Cl^- ions can dissolve twin and single crystals and passivate the Ag{111} side of the AgNS, resulting in a sub-circular nanosheet.[32,33] In this work, due to the high surface activity of the tips of AgNSs, the free Cl^- ions will recombine the Ag^+ at the tips of the AgNSs to reform AgCl, thereby causing AgNSs turn into AgNDs.

The morphology and microstructure of AgNDs obtained were further characterized by TEM, and the inset shows the corresponding electron diffraction patterns (Figure 4a). The size of AgNDs is ∼500 nm, and their edges and corners

https://doi.org/10.1021/acsomega.2c01928
ACS Omega 2022, 7, 28860−28865

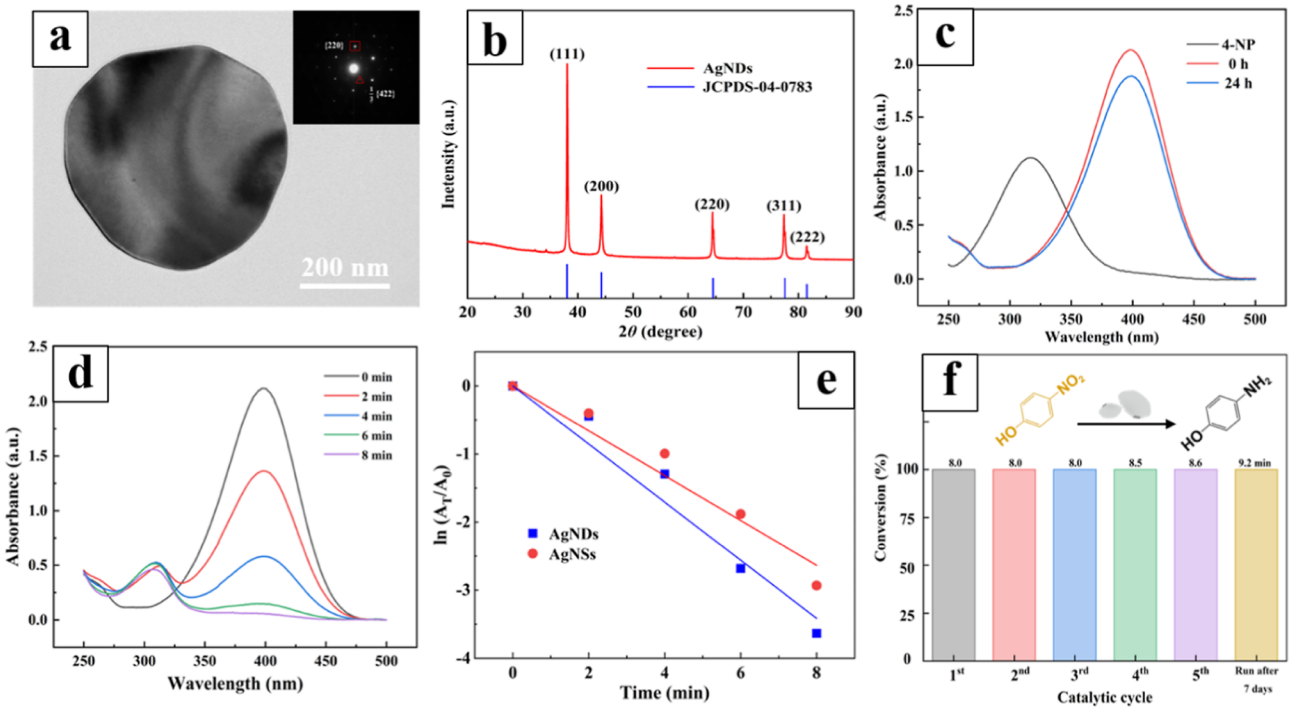

Figure 4. (a) TEM image of AgNDs; the inset shows the electron diffraction pattern. (b) XRD pattern of AgNDs. (c) UV−vis spectra of 4-NP solution before and after adding $NaBH_4$. (d) Successive UV−vis spectra of 4-NP solution with $NaBH_4$ catalyzed by AgNDs. (e) Catalytic rate constant graph of AgNSs and AgNDs. (f) Recycling tests of the AgND catalyst for five successive runs and a run after a long storage time (around 7 days after the catalyst synthesis) for 4-NP. The reaction conditions of (e) and (f): [4-NP] = 0.1×10^{-6} M, Ag = 0.54×10^{-4} g, and [$NaBH_4$] = 0.1×10^{-3} M.

become rounded. In addition, it can be seen from Figure S3d that there is a PVP capping layer of several nanometers on the edge of the AgNDs. The square spot in the illustration allows {220} reflection, and Figure S3b shows the lattice spacing to be 1.44 Å. The triangular (Figure S3a) spot corresponds to the theoretically prohibited 1/3 {422} reflection, and its fringe spacing is 2.5 Å (Figure S3c). All the results reveal that the crystal structure of AgNDs is a typical face-centered cubic (fcc) structure.

The XRD pattern of AgNDs is shown in Figure 4b. There are four strong diffraction peaks and one weak diffraction peak at 38.1, 44.2, 64.4, 77.4, and 81.5°, corresponding to the (111), (200), (220), (311), and (222) reflections of the fcc structure of silver (JCPDS 04-0783), respectively. It is worth noting that the intensity of the (111) diffraction peak is almost the sum of the intensities of other diffraction peaks, indicating that the synthesized AgNDs are mainly composed of (111) crystal planes, which is well consistent with the results of SEM and TEM.

As is known, the UV−vis characteristic peak of 4-NP is around 400 nm.[34,35] As seen from Figure 4c, the characteristic peak of 4-NP dropped slowly even after 24 h in absence of a catalyst. However, after adding 0.054 mg of AgNDs, the peak intensity of 4-NP dropped sharply within 8 min, and a new peak arose at ∼300 nm at the same time, indicating the formation of 4-AP (Figure 4d). The catalytic rates of AgNSs and AgNDs are shown in Figure 4e. The linear relationship between $\ln(A_T/A_0)$ and the reaction time was further obtained, where A_T and A_0 are the 4-NP concentrations at times T and 0, respectively, and the rate constants of the catalysts were evaluated using pseudo-first-order kinetics. The calculated catalytic rate constant (k) of AgNDs is 0.00792 s^{-1}, and the activity factor (K) is 146.66 $s^{-1}{\cdot}g^{-1}$. The specific surface area (BET) analysis test results of AgNDs and AgNSs showed that AgNDs have a larger specific surface area (Table 1 and Figure S4). As is known, the catalytic performance is closely related with the surface of the catalyst. Therefore, AgNDs in this work may expose more catalytically active sites, which make the catalytic activity better than that of AgNSs. As compared with previously reported metal catalysts, AgNDs in this work also showed higher catalytic activity (Table 2). It is believed that

Table 1. BET Surface Areas of the Samples

sample	BET surface area (m^2/g)
AgNSs	2.7054
AgNDs	3.2301

Table 2. Comparison of Rate Constants and Activity Factors of Different Catalysts for the Reduction of 4-NP

sample	quality/g	rate constant (k)/s^{-1}	activity factor (K)/$s^{-1}{\cdot}g^{-1}$	reference
Ag/Fe_2O_3 NPs	0.005	0.01438	2.87	5
Au/Co_3O_4	0.001	0.1638	218.84	19
Ag-NPs/C	0.001	0.00169	1.69	20
Fe_3O_4@CS_AgNi	0.0008	0.0093	11.66	22
CuNPs	0.000052	0.0071	136.54	23
AgNPs	0.0005	0.00705	6.741	26
Fe_3O_4@SiO_2-NH_2−Au	0.003	0.0625	20.83	35
AgNDs	0.000054	0.00792	146.66	this work

https://doi.org/10.1021/acsomega.2c01928
ACS Omega 2022, 7, 28860−28865

the polygonal AgNSs prepared in advance in this study have sharp corners and straight sides. When these sharp corners and edges are Cl^--etched, AgNDs become blunt, thus likely exposing and providing more effective catalytic sites for the reduction of 4-NP (Figure 4e).[36]

To further evaluate the stability and recyclability of the catalyst for 4-NP reduction, the catalyst used was collected and then applied directly for the next cycle. The results in Figure 4f show a slight increase in reduction time even after five cycles (8.0−8.6 min for 4-NP), probably due to sampling loss. It demonstrated that the catalyst almost did not undergo any appreciable change in its activity. More remarkably, the catalyst efficiently carried out 100% conversion of 4-NP within 9.2 min even after 7 days of storage.

4. CONCLUSIONS

In summary, the one-step synthesis of AgNDs in DMF by using $FeCl_3$ as an additive has been reported. Under the synergetic reduction of DMF and Fe^{2+} ions, Ag^+ ions are gently reduced into Ag^0 atoms and silver seed crystals, then inducing the formation of AgNSs in the presence of PVP molecules. Subsequently, the overmuch Cl^- ions in the system continuously recombine the Ag^+ at the tips of AgNSs, finally causing the polygonal AgNSs turn into AgNDs. Additionally, AgNDs showed considerable catalytic activity in the reduction of 4-NP to 4-AP.

■ ASSOCIATED CONTENT

Supporting Information

The Supporting Information is available free of charge at https://pubs.acs.org/doi/10.1021/acsomega.2c01928.

Samples prepared under various reaction conditions, SEM images of different samples, HRTEM images of AgNSs and AgNDs, and BET surface area plots of AgNSs and AgNDs (PDF)

■ AUTHOR INFORMATION

Corresponding Authors

Hongwei Yang − *State Key Laboratory of Advanced Technologies for Comprehensive Utilization of Platinum Metals, Kunming Institute of Precious Metals, 650106 Kunming, People's Republic of China*; orcid.org/0000-0002-0527-1294; Email: nanolab@ipm.com.cn

Hao Cui − *State Key Laboratory of Advanced Technologies for Comprehensive Utilization of Platinum Metals, Kunming Institute of Precious Metals, 650106 Kunming, People's Republic of China*; Email: cuihao@ipm.com.cn

Authors

Jie Chen − *State Key Laboratory of Advanced Technologies for Comprehensive Utilization of Platinum Metals, Kunming Institute of Precious Metals, 650106 Kunming, People's Republic of China*

Linlin He − *State Key Laboratory of Advanced Technologies for Comprehensive Utilization of Platinum Metals, Kunming Institute of Precious Metals, 650106 Kunming, People's Republic of China*

Zhengyang Fan − *State Key Laboratory of Advanced Technologies for Comprehensive Utilization of Platinum Metals, Kunming Institute of Precious Metals, 650106 Kunming, People's Republic of China*

Huaming Mao − *State Key Laboratory of Advanced Technologies for Comprehensive Utilization of Platinum Metals, Kunming Institute of Precious Metals, 650106 Kunming, People's Republic of China*

Yu Ren − *State Key Laboratory of Advanced Technologies for Comprehensive Utilization of Platinum Metals, Kunming Institute of Precious Metals, 650106 Kunming, People's Republic of China*

Jungang Yin − *State Key Laboratory of Advanced Technologies for Comprehensive Utilization of Platinum Metals, Kunming Institute of Precious Metals, 650106 Kunming, People's Republic of China*

Wei Dai − *State Key Laboratory of Advanced Technologies for Comprehensive Utilization of Platinum Metals, Kunming Institute of Precious Metals, 650106 Kunming, People's Republic of China*

Complete contact information is available at: https://pubs.acs.org/10.1021/acsomega.2c01928

Notes

The authors declare no competing financial interest.

■ ACKNOWLEDGMENTS

This work was supported by the National Natural Science Foundation of China (grant no. 21761016), the Young and Middle-aged Academic and Technical Leaders Reserve Talents Program of Yunnan Province (grant no. 2017HB060), the Major R&D Project of Yunnan Province (grant nos. 202002AB080001-1 and 202102AB080008-5), and the Ten Thousand Talents Plan-Young Top Talent Program of Yunnan Province.

■ REFERENCES

(1) Ponomarev, V. A.; Sheveyko, A. N.; Permyakova, E. S.; Lee, J.; Voevodin, A. A.; Berman, D.; Manakhov, A. M.; Michlíček, M.; Slukin, P. V.; Firstova, V. V.; Ignatov, S. G.; Chepkasov, I. V.; Popov, Z. I.; Shtansky, D. V. TiCaPCON-supported Pt- and Fe-based nanoparticles and related antibacterial activity. *ACS Appl. Mater. Interfaces* **2019**, *11*, 28699−28719.

(2) Lu, X.; Hou, J.; Yang, K.; Zhu, L.; Xing, B.; Lin, D. Binding force and site-determined desorption and fragmentation of antibiotic resistance genes from metallic nanomaterials. *Environ. Sci. Technol.* **2021**, *55*, 9305−9316.

(3) Jiang, T.; Chen, G.; Tian, X.; Tang, S.; Zhou, J.; Feng, Y.; Chen, H. Construction of long narrow gaps in Ag nanoplates. *J. Am. Chem. Soc.* **2018**, *140*, 15560−15563.

(4) Luneau, M.; Guan, E.; Chen, W.; Foucher, A. C.; Marcella, N.; Shirman, T.; Verbart, D. M. A.; Aizenberg, J.; Aizenberg, M.; Stach, E. A.; Madix, R. J.; Frenkel, A. I.; Friend, C. M. Enhancing catalytic performance of dilute metal alloy nanomaterials. *Commun. Chem.* **2020**, *3*, 46.

(5) Wang, N.; Zeng, S.; Yuan, H.; Huang, J. Morphology-dependent interfacial interactions of Fe_2O_3 with Ag nanoparticles for determining the catalytic reduction of p-nitrophenol. *J. Environ. Sci.* **2020**, *92*, 1−10.

(6) Wu, Y.; Wang, D.; Li, Y. Understanding of the major reactions in solution synthesis of functional nanomaterials. *Sci. China Mater.* **2016**, *59*, 938−996.

(7) Shi, Y.; Lyu, Z.; Zhao, M.; Chen, R.; Nguyen, Q. N.; Xia, Y. Noble-metal nanocrystals with controlled shapes for catalytic and electrocatalytic applications. *Chem. Rev.* **2021**, *121*, 649−735.

(8) Chen, Y.; Fan, Z.; Zhang, Z.; Niu, W.; Li, C.; Yang, N.; Chen, B.; Zhang, H. Two-dimensional metal nanomaterials: synthesis, properties, and applications. *Chem. Rev.* **2018**, *118*, 6409−6455.

(9) Rycenga, M.; Cobley, C. M.; Zeng, J.; Li, W.; Moran, C. H.; Zhang, Q.; Qin, D.; Xia, Y. Controlling the synthesis and assembly of silver nanostructures for plasmonic applications. *Chem. Rev.* **2011**, *111*, 3669−3712.
(10) Maillard, M.; Giorgio, S.; Pileni, M. P. Silver nanodisks. *Adv. Mater.* **2002**, *14*, 1084−1086.
(11) Kim, J.; Lee, S. W.; Kim, M. H.; Park, O. O. Zigzag-shaped silver nanoplates: synthesis via ostwald ripening and their application in highly sensitive strain sensors. *ACS Appl. Mater. Interfaces* **2018**, *10*, 39134−39143.
(12) Weng, G.; Feng, Y.; Zhao, J.; Li, J.; Zhu, J.; Zhao, J. Size dependent SERS activity of Ag triangular nanoplates on different substrates: glass vs paper. *Appl. Surf. Sci.* **2019**, *478*, 275−283.
(13) Khan, A. U.; Zhou, Z.; Krause, J.; Liu, G. Poly-(vinylpyrrolidone)-free multistep synthesis of silver nanoplates with plasmon resonance in the near infrared range. *Small* **2017**, *13*, 1701715−1701722.
(14) Chen, S.; Fan, Z.; Carroll, D. L. Silver nanodisks: synthesis, characterization, and self-assembly. *J. Phys. Chem. B* **2002**, *106*, 10777−10781.
(15) Tang, B.; An, J.; Zheng, X.; Xu, S.; Li, D.; Zhou, J.; Zhao, B.; Xu, W. Silver nanodisks with tunable size by heat aging. *J. Phys. Chem. C* **2008**, *112*, 18361−18367.
(16) Neethu, T.; Ethayaraja, M. An experimental investigation on tuning the edge length of Ag nanoplates. *The International Conference on Emerging Trends in Engineering Yukthi-21*, Government Engineering College Kozhikode, 2021Available at SSRN 4017800.
(17) Pastoriza-Santos, I.; Liz-Marzán, L. M. Synthesis of silver nanoprisms in DMF. *Nano Lett.* **2002**, *2*, 903−905.
(18) Kim, M. H.; Yoon, D. K.; Im, S. H. Growth pathways of silver nanoplates in kinetically controlled synthesis: bimodal versus unimodal growth. *RSC Adv.* **2015**, *5*, 14266−14272.
(19) Yang, Y.; Mao, Y.; Wang, B.; Meng, X.; Han, J.; Wang, C.; Yang, H. Facile synthesis of cubical Co_3O_4 supported Au nanocomposites with high activity for the reduction of 4-nitrophenol to 4-aminophenol. *RSC Adv.* **2016**, *6*, 32430−32433.
(20) Tang, S.; Vongehr, S.; Meng, X. Carbon spheres with controllable silver nanoparticle doping. *J. Phys. Chem. C* **2010**, *114*, 977−982.
(21) Andreou, D.; Iordanidou, D.; Tamiolakis, I.; Armatas, G. S.; Lykakis, I. N. Reduction of nitroarenes into aryl amines and N-aryl hydroxylamines via activation of $NaBH_4$ and ammonia-borane complexes by Ag/TiO2 catalyst. *Nanomaterials* **2016**, *6*, 54.
(22) Antony, R.; Marimuthu, R.; Murugavel, R. Bimetallic nanoparticles anchored on core−shell support as an easily recoverable and reusable catalytic system for efficient nitroarene reduction. *ACS Omega* **2019**, *4*, 9241−9250.
(23) Li, Y.; Fan, Z.; Yang, H.; Yuan, X.; Chao, Y.; Li, Y.; Wang, C. Bromine anion-induced synthesis of copper nanoplates and their recyclable catalytic activity towards 4-nitrophenol reduction. *CrystEngComm* **2020**, *22*, 7786−7789.
(24) Chiou, J.-R.; Lai, B.-H.; Hsu, K.-C.; Chen, D.-H. One-pot green synthesis of silver/iron oxide composite nanoparticles for 4-nitrophenol reduction. *J. Hazard. Mater.* **2013**, *248−249*, 394−400.
(25) Zhang, W.; Tan, F.; Wang, W.; Qiu, X.; Qiao, X.; Chen, J. Facile, template-free synthesis of silver nanodendrites with high catalytic activity for the reduction of p-nitrophenol. *J. Hazard. Mater.* **2012**, *217−218*, 36−42.
(26) Jin, R.; Cao, Y.; Mirkin, C. A.; Kelly, K. L.; Schatz, G. C.; Zheng, J. G. Photoinduced conversion of silver nanospheres to nanoprisms. *Science* **2001**, *294*, 1901−1903.
(27) Thomas, N.; Mani, E. Mechanism and modeling of poly-[vinylpyrrolidone] (PVP) facilitated synthesis of silver nanoplates. *Phys. Chem. Chem. Phys.* **2018**, *20*, 15507−15517.
(28) Wiley, B.; Sun, Y.; Xia, Y. Polyol synthesis of silver nanostructures: control of product morphology with Fe (II) or Fe (III) species. *Langmuir* **2005**, *21*, 8077−8080.
(29) Korte, K. E.; Skrabalak, S. E.; Xia, Y. Rapid synthesis of silver nanowires through a CuCl-or $CuCl_2$-mediated polyol process. *J. Mater. Chem.* **2008**, *18*, 437−441.
(30) Zeng, J.; Xia, X.; Rycenga, M.; Henneghan, P.; Li, Q.; Xia, Y. Successive deposition of silver on silver nanoplates: lateral versus vertical growth. *Angew. Chem., Int. Ed.* **2011**, *50*, 244−249.
(31) Gatemala, H.; Pienpinijtham, P.; Thammacharoen, C.; Ekgasit, S. Rapid fabrication of silver microplates under an oxidative etching environment consisting of O_2/Cl^-, NH_4OH/H_2O_2, and H_2O_2. *CrystEngComm* **2015**, *17*, 5530−5537.
(32) Dong, M.; Fu, R.; Min, H.; Zhang, Q.; Dong, H.; Pan, Y.; Sun, L.; Wei, W.; Qin, M.; Zhu, Z.; Xu, F. In situ liquid cell transmission electron microscopy investigation on the dissolution-regrowth mechanism dominating the shape evolution of silver nanoplates. *Cryst. Growth Des.* **2021**, *21*, 1314−1322.
(33) Tang, B.; Xu, S.; An, J.; Zhao, B.; Xu, W.; Lombardi, J. R. Kinetic effects of halide ions on the morphological evolution of silver nanoplates. *Phys. Chem. Chem. Phys.* **2009**, *11*, 10286−10292.
(34) Bharadwaj, K. K.; Rabha, B.; Pati, S.; Choudhury, B. K.; Sarkar, T.; Gogoi, S. K.; Kakati, N.; Baishya, D.; Kari, Z. A.; Edinur, H. A. Green synthesis of silver nanoparticles using diospyros malabarica fruit extract and assessments of their antimicrobial, anticancer and catalytic reduction of 4-nitrophenol (4-NP). *Nanomaterials* **2021**, *11*, 1999−2023.
(35) Bhaduri, K.; Das, B. D.; Kumar, R.; Mondal, S.; Chatterjee, S.; Shah, S.; Bravo-Suárez, J. J.; Chowdhury, B. Recyclable Au/SiO_2-shell/Fe_3O_4-core catalyst for the reduction of nitro aromatic compounds in aqueous solution. *ACS Omega* **2019**, *4*, 4071−4081.
(36) Tan, T.; Zhang, S.; Wang, C. Branched Ag nanoplates: synthesis dictated by suppressing surface diffusion and catalytic activity for nitrophenol reduction. *CrystEngComm* **2017**, *19*, 6339−6346.

https://doi.org/10.1021/acsomega.2c01928
ACS Omega 2022, 7, 28860−28865